Modeling of Random Nanostructures Based on SEM Images and Analysis of Resulting RF Performance

K. Neumann[1], J. Moeller[1], L. Kuehnel[2], A. Rennings[1], N. Benson[2], R. Schmechel[2], D. Erni[1]

[1]General and Theoretical Electrical Engineering (ATE), University of Duisburg-Essen, and CENIDE – Center for Nanointegration Duisburg-Essen, D-47048, Duisburg, Germany
[2]Institute for Nanostructures and Technology (NST), University of Duisburg-Essen, and CENIDE – Center for Nanointegration Duisburg-Essen, D-47048, Duisburg, Germany

Introduction

In the last few years printable electronics has gained a great deal of interest since it promises mechanical flexibility and extremely low production costs. One approach to achieve printable electronic devices relies on the usage of specific inks containing e.g. dispersed semiconductor nanoparticles, where the latter are then apt to further processing steps [1]. In this work, doped silicon (Si) nanoparticles are printed on a metal substrate and then fuzed by subsequent laser sintering. Due to a detailed balance between melting, cohesive forces and, thermal cooling, the nanoparticles self-organize themselves to form crystalline Silicon (c-Si) cone- like nanostructures, representing a valuable structural predecessor to e.g. printable high-speed Schottky diodes. However not all Si nanoparticles have enough mass to achieve cone-like structures and instead form hemispherical droplets which cannot be utilized as diodes. The planar distribution of these droplets and the self-assembled c-Si cones that are embedded in a dielectric background medium can be treated like a planar random surface. Therefore, the goal of this work is to extract the random morphology and its stochastic properties in order to create an accurate numerical representation within COMSOL Multiphysics®. The model is then used to extract the parasitic capacitances of future cone-like Schottky diodes. By analyzing the set of Scanning Electron Microscopy (SEM) images of the c-Si cones, a mathematical representation of the shapes can be retrieved. We use polynomial functions to fit the surface of each c-Si cone together with a morphing functionality that enables the representation of non-symmetric cone shapes. To model the random nature of the cone distribution and droplet distribution, hence of the planar random surface, a probability density function is defined for all parameters defining shape and position of the nanostructures. Based on these functions we can then use the LiveLink™ for MATLAB® module to generate random c-Si cone settings (i.e. realistic random surfaces) within COMSOL Multiphysics®, which are supposed to exhibit the same statistic distributions as the fabricated ones. The influence of each stochastic parameter onto the complex admittance is analyzed by running batch simulations using the Electric Currents and Electrostatics physics within the AC/DC module. The derived capacitances and conductances provide an important measure for the envisaged technology regarding its applicability to e.g. printable RFID tags and flexible lowest-cost radio frequency (RF) electronics, as they limit the upper bound of the operation frequency (i.e. cut-off frequency). The cut-off frequency represents the transition frequency where the displacement current in the dielectric background starts predominating the electric current in the c-Si cone. Figure 1 shows an utilization example of the Schottky diodes as an RF-device. The c-Si cones (i.e. the diodes) are sandwiched between two metal contacts and embedded in a dielectric. The box in red indicates the simulation region which is modeled in COMSOL Multiphyics®.

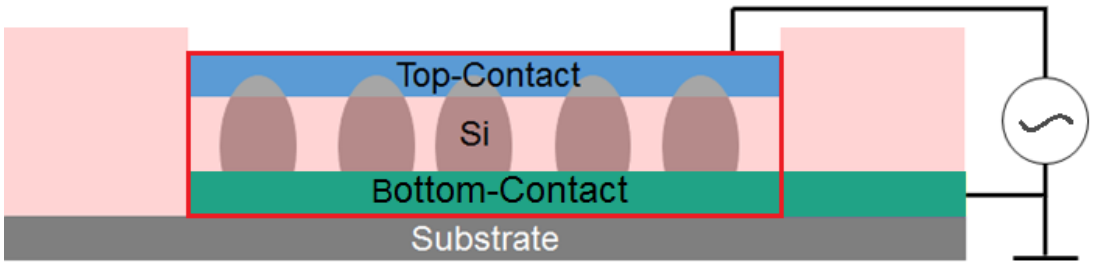

Figure 1: Schematic representation of printable Schottky diode device for radio frequency applications.

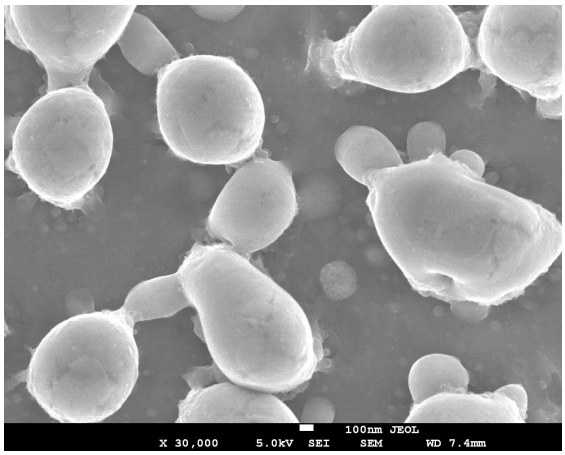

Figure 2: Top view Scanning Electron Microscope image of c-Si cones

SEM Image Analysis

Due to their shape and orientation to each other, the nanostructures exhibit a parasitic capacitance which limits the high-speed switching behavior. To estimate these limits the geometries of the cones and droplets have to be modeled properly. By manipulating the SEM images in a certain way (see [2][3] as a reference), the geometric features can be extracted. In this work, the image analysis is done in MATLAB with use of the Image Processing Toolbox [4].

Top View Analysis

An example of a SEM image from the top view is drawn in Figure 2. It can be seen that the structures vary in shape and height. Some structures exhibit strong white contours, which will be referred to as cones, others appear blurred – they will be called droplets. The Top View Analysis has two objectives. One is to identify the cones and on the other hand to evaluate the size of the droplets. It has to be stated that the top view SEM images don't contain any height information, hence these information has to be extracted from the Cross Section View Analysis. Nonetheless the footprint of the cones and the size of the hemispherical droplets can be retrieved. Figure 3 shows the steps taken to access the geometric information. At first, to extract the cone footprints, a threshold filter is applied (Fig. 3 (a)). A combination of a morphological opening step [5] followed by an area filter is used to eliminate small pixel clusters (Fig. 3 (b)). With the use of the boundary detection methods [6], separated objects and their edges are identified (Fig. 3 (c)). The position of each cone is calculated by taking the geometric average value of all edge pixel coordinates. After that each edge pixel is then transformed in a polar coordinate formulation with the cone position as its origin. With this type of formulation, a function of the radius or distance from the center to the edge is determined as a function of the azimuth angle. To reduce the effects of artifacts, this function is filtered by a low pass (Fig. 3 (d)). For the extraction of the smaller droplets, the cone footprints are removed from the image and a similar approach as previously was used. Again, a threshold filter, the area filter and the boundary detection method is applied with slight different parameters (Fig. 3 (e - g). Also, the radius function is now constant and calculated by taking the average distance between center point and each edge pixel (Fig. 3 (h)).

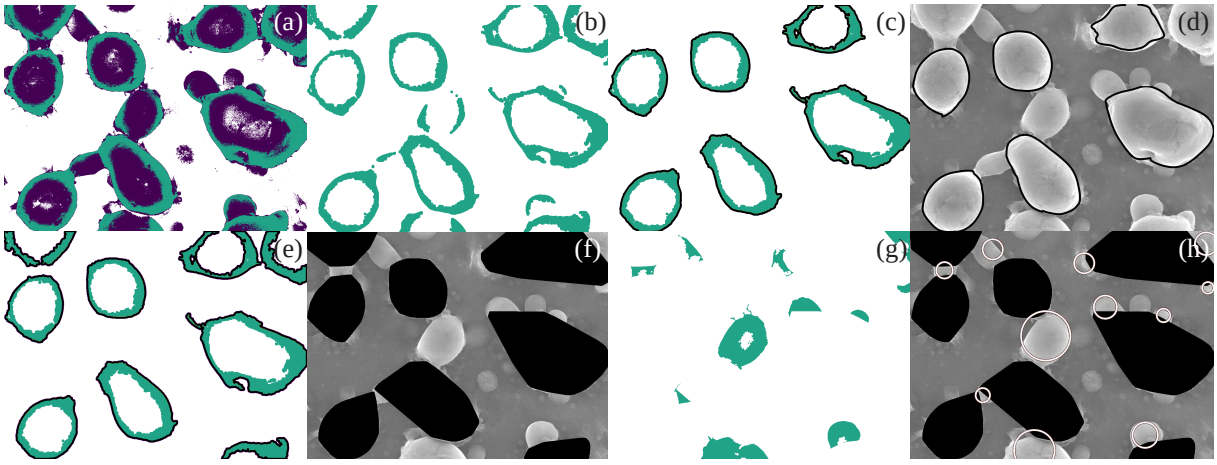

Figure 3: Steps of shape detection process. Images (a) to (d) refer to the extraction of the cone footprints. Images (e) to (h) show the process of detecting smaller droplets. (a) Threshold filter. (b) Morphological opening. (c) Area filter and boundary detection. (d) Low pass filter and finished footprint detection. (e) Same as step (c) but with different parameters. (f) Bigger cone footprints are removed from the image. (g) Threshold filter. (h) Boundary detection and calculation of mean radius.

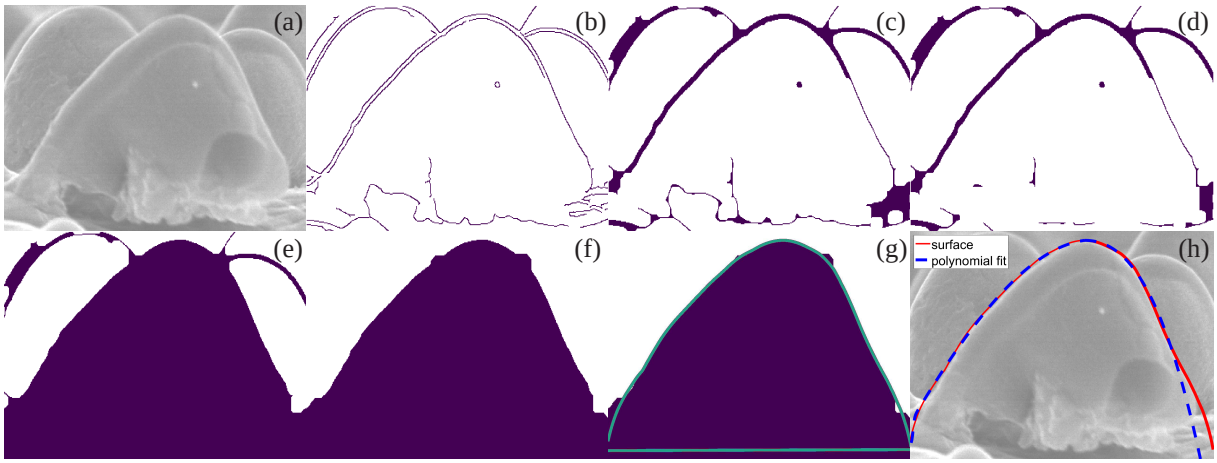

Figure 4: Process of shape function extraction. (a) Picture of one cone. (b) Edge detection filter. (c) Morphological closing. (d) Threshold filter. (e) Filling of center region. (f) Morphological opening. (g) Boundary detection. (h) Fitting of boundary pixels.

Cross Section View Analysis

To obtain the height distribution and shape functions of the cones, 8 cross-cut images are analyzed. From these 8 images 25 sub-images are created by hand, showing one isolated cone each. In Figure 4 the process of extracting the surface for one cone is shown. At first the edge detection algorithm "Canny" [7] is applied (Fig. 4 (b)). The result, however, is an image in which the edges are thin and in some respect unconnected. Therefore the image is morphologically closed (Fig. 4 (c)) to get continuous lines and edges. In some cases the Canny algorithm detects too many edges in the center region which would compromise later steps. Thus these edges are deleted (Fig. 4 (d)), before the center region is filled (Fig. 4 (e)). To eliminate the edges of the cones which lay behind the cone of interest, an opening algorithm is applied (Fig. 4 (f)). Now the boundary detection method in combination with a spatial low pass filter can be used to detect the surface of the cone (Fig. 4 (g)). Having the pixels of the cone's border, a mathematical description of the cone shape is now possible. In these images, 25 cones can be identified and their shape can be fitted by combining a polynomial and a sigmoid function such as equation (1).

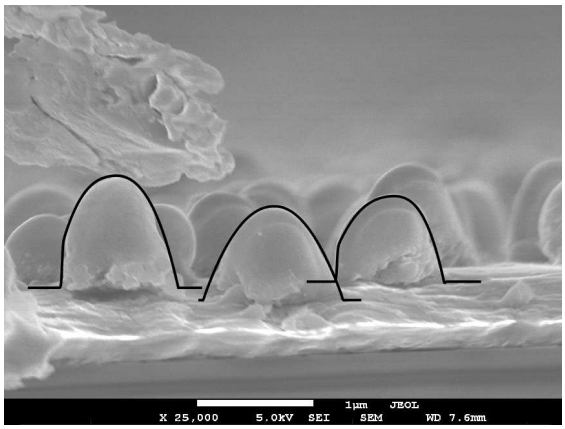

Figure 5: Example of cross section image with fitted shape functions drawn in black.

$$y(x) = (a \cdot x^3 + b \cdot x^2 + c \cdot x + d) \cdot \frac{1}{1 + e^{x+w}} \quad (1)$$

where $y(x)$ approximates the surface in dependence of the x-coordinate and a, b, c, d and w are the fitting coefficients. The sigmoid function is needed to limit the output of the polynomial and to get a smooth transition between cone surface and substrate. However, it is beneficial to split up the cone surface formulation in two halves. The highest point of each cone surface is determined and defined as the center i.e. $x = 0$. As a result, the coefficient d is equal to the height of the cone in pixels. It is determined by calculating the difference of highest and lowest y-coordinate of the edge pixels. Since d is computed, it no longer has to be derived from the fitting process. For each half the given equation (1) has to be applied. That means the pixels to the left and to the right of the center have to be fitted separately. It has proven beneficial to add a weight to the surface points according to equation (2).

$$weights = x^{-2} \quad (2)$$

By weighting the points in this way, more importance is attributed to the center of the cones. Figure 5 shows the results of the fitting process. The two surface functions of each cone are drawn onto the according surfaces.

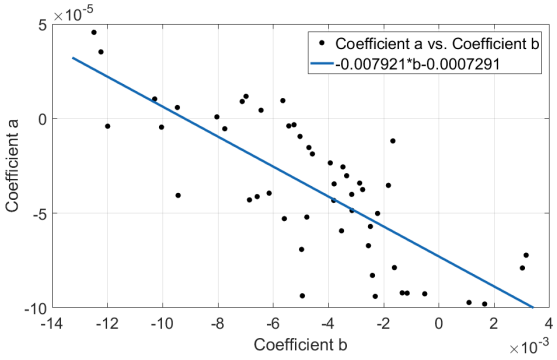

Figure 6: Correlation between coefficient a and b. Linear regression function in blue.

3D Structures

By fitting the polynomials onto the surface of the cones, one has to assume that the coefficients exhibit some correlation to each other, which has to be taken into account for the random generation of the cones. The respective coefficients of the cones are combined into a vector. Thus, the correlation of one coefficient to another can be easily determined. Figure 6 shows first coefficient a plotted against the second coefficient b and the resulting regression line. By subtracting this regression line from the coefficient vector the correlation between a and b is suppressed. Now the probability density functions (PDF) for each coefficient can be determined by calculating the mean value and the standard deviation. In this work it is assumed that each coefficient follows a normal distribution. The first step for creating random cones is to generate random coefficient numbers with the according PDF. For the coefficients a and c the correlation has to be recreated by adding the correlation function which is, in good approximation, the regression line. With the random coefficients, the surface curve for the left and right half can be generated using the shape function given in equation (1). The second step involves the rotation of the surface curves along the z-axis by 180 degrees. To avoid discontinuities the left and right polynomial functions are morphed into each other depending on the rotation angle using another sigmoid function $\mu(\alpha)$:

$$\mu(\alpha) = \frac{1}{1 + 3 \cdot e^{\alpha + \frac{\pi}{2}}} \tag{3}$$

The surface can now be described in polar coordinates with equation (4).

$$\begin{aligned} z(r', \alpha) = \mu(\alpha) \cdot y_{left}(r') \\ +(1 - \mu(\alpha)) \cdot y_{right}(r') \end{aligned} \tag{4}$$

Here y_{left} corresponds to the left half of the surface shape equation [cf. eq. (1)]. Whereas y_{right} resembles the right half. It is obvious that this approach introduces an axial symmetry which is unlikely to happen in the physical world. Therefore this rotation has to be morphed by the footprints obtained by the Top View Analysis. These footprints are also given in a polar coordinate formulation. Where each point is described by the angle and distance to the cone's center point. By inserting the respecting distance into r' of equation (4) an asymmetric surface is created which should exhibit the same geometric properties as the real cones. Figure 7 shows an example of random surface functions and the resulting random surface. To import these surfaces into COMSOL, the surface information and other properties like the span of the surface are exported into a spreadsheet file.

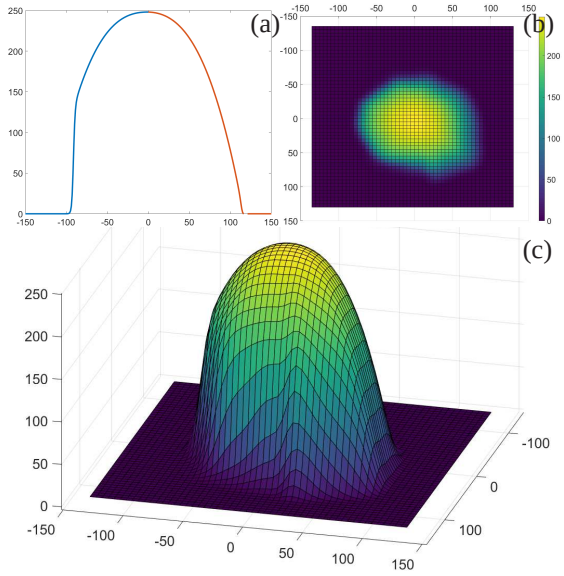

Figure 7: Random cone generation within MATLAB. (a) Plot of left and right surface function. (b) Top-View of generated surface. (c) 3D-View of generated surface.

COMSOL Import and Simulation Setup

The surfaces generated in the last section can be imported into COMSOL Multiphyics by the Interpolation function. A parametric surface is used to call

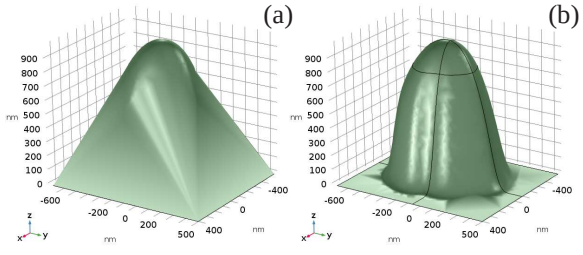

Figure 8: Imported (random) surface in COMSOL. (a) first import. (b) Surface after partitioning.

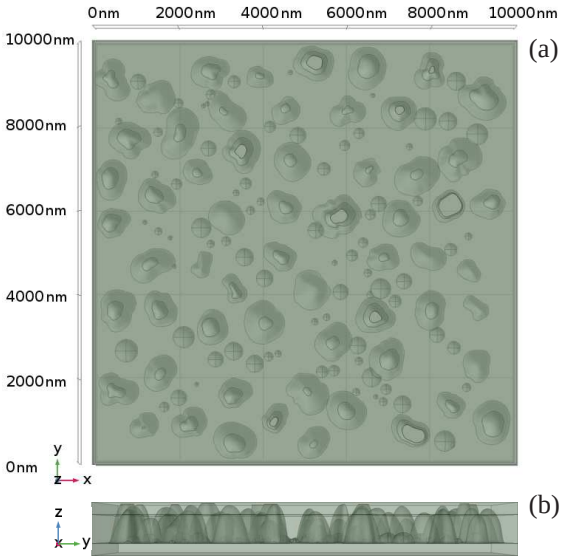

Figure 9: 3D Model of the ensemble of random cones and droplets in COMSOL Multiphysics®: (a) top view. (b) side view.

this function. However the standard implementation is not sophisticated enough to exactly represent the surfaces, as can be seen in Figure 8 (a). The COMSOL surface tries to approximate the given interpolation function, however some artifacts can arise. Increasing the number of knots doesn't help and just consumes more time to build. A more convenient way to help COMSOL to get the right surface representation, is to partition the surface. Figure 8 (b) shows the surface after its outer edges have been partitioned and also after the surface is cut by work planes along the x- and y- axis. It is evident that the surface representation is much more sophisticated now. To prepare the virtual cone for the simulation another work plane cut has to be applied in the xy-plane but with some displacement in the z-axis. This cut will represent the top contact for the RF-devices. It should be noted that this is only possible after cutting the surface along the x- and y- axis. Finally the parametric surface is converted into a solid and some unwanted edges are deleted. This process is repeated for each generated surface and then stored in an individual .mphbin file, which can be imported by the COMSOL simulation model. For the simulation a three-layered box is created which represent the two metal contacts and the dielectric. The cones are

	Cones	Droplets
Mean Height	921 nm	129 nm
Standard Deviation	153 nm	67 nm

Table 1: Geometric size distributions retrieved from the SEM image analysis.

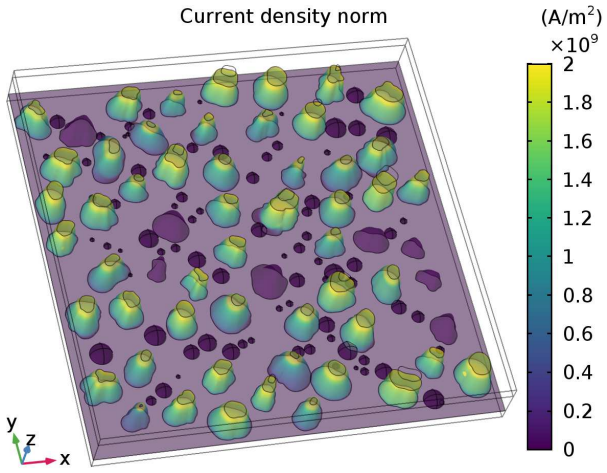

Figure 10: Surface plot of the current density norm in COMSOL Multiphysics®.

placed on the first layer and depending on the height distribution reach into the third top layer. Figure 9 shows the simulation model from the top. With the LiveLink™ for MATLAB® module the cones and droplets can be placed randomly within the boundaries of the model. However, it is ensured that they maintain a minimum distance from each other. The standard Si material of COMSOL Multiphysics® is extended by a custom function to achieve a conductivity which is dependent on the doping concentration [8]. In this work an n-doping concentration of $5 \cdot 10^{16}$ cm^{-3} is used. To estimate the total equivalent circuit capacitance, the bottom and top layer of the simulation box are defined as terminal within the Electrostatics and Electric Currents modules. To reach cut-off frequencies above 10 GHz the device area has to be small, in the range of few hundred $\mu\mathrm{m}^2$ [9]. In this work the device is chosen to be 10 $\mu\mathrm{m}$ by 10 $\mu\mathrm{m}$. 60 diodes and 78 droplets have to be distributed across that area to obtain the same structure count per $\mu\mathrm{m}^2$ as seen in the top view SEM images. The standard size distributions obtained from the SEM image analysis can be found in table 1. The contact height, i.e. the distance between the lower and upper metal contact, is set to 800 nm, as this number should provide a certain degree of assurance that even smaller cones are in contact with the top metal.

Results

As a first test the Electric Currents module is run for a single frequency. By looking at the current densities, which are shown in Figure 10, one can certify that the model works in the expected way. Most of the cones reach from bottom to top contact and hence can carry current. Some of them are too small, like

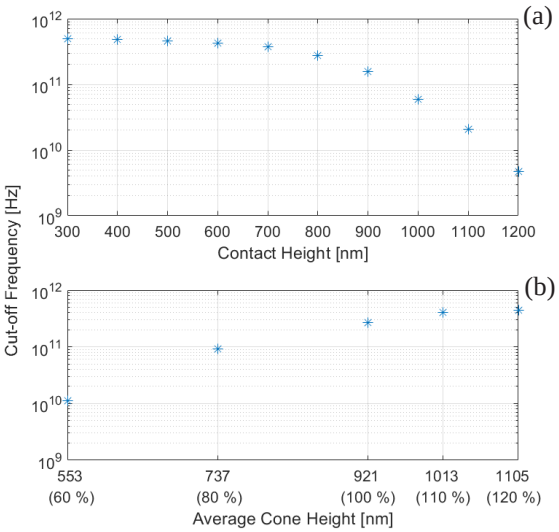

Figure 11: Cut-off frequency plotted against: (a) contact height and (b) average cone height.

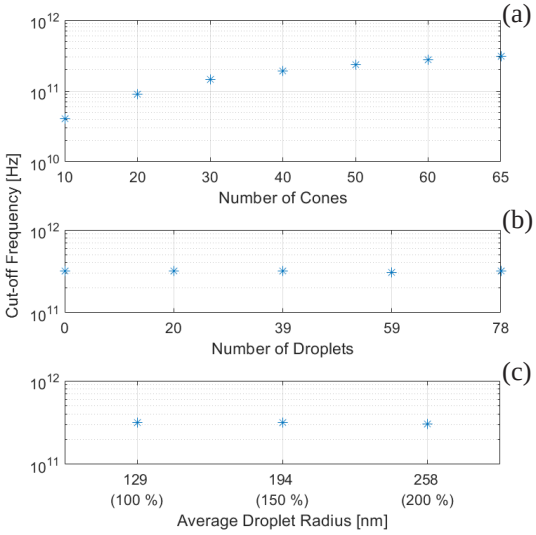

Figure 12: (a) Different diode counts (b) Different droplet counts (c) Different average droplet radius and resulting cut-off frequency.

the droplets, so they can't act as potential diodes. Now different studies regarding the influence onto the cut-off frequency of different geometric parameters are conducted. For evaluating the cut-off frequency the Electric Currents module is run in a frequency sweep from 10^9 Hz to 10^{12} Hz. In this paper the cut-off frequency means the frequency where the imaginary part of the admittance equals the real part. From that frequency on the current will be dominated by the displacement current and the diode looses its rectification ability. It has to be noted that the model only contains the capacitances and resistances that arise from the geometry. Capacities due to charge depletion or other semiconductor-related effects are not considered and therefore the cut-off frequency estimate is too high as it values only the passive diode structure. Nevertheless, it is possible to analyze the parasitic components of the geometry and minimize them in order to achieve the highest possible cut-off frequency. In the first study the influence of the contact height is determined, which is shown in Figure 11 (a). If the distance is too high, the cut-off frequency decreases, as fewer cones can work as diodes. Nonetheless, if the contact height decreases the cut-off frequency saturates, as the resistance drops but the capacitance due to the plate capacitor rises. This leads to the conclusion that for each shape and geometry distribution of the RF-device, an optimal contact height exists, which can be for the first time estimated with this comprehensive model. If, on the other hand, the mean height of the cones is varied instead of the contact height, a slightly different pattern appears as displayed in Figure 11 (b). Again as the cone height increases, the cut-off frequency increases as well because more cones are in contact with the top metal and the area of these contacts rises. Similar results are retrieved if the the number of the cones is analyzed. In Figure 12 (a) it can be seen that, as the count of the cones rises, the cut-off frequency rises. However, a saturation effect occurs. Surprisingly, the droplets don't have any influence onto the cut-off frequency. The cut-off frequency remains almost constant as the droplets are gradually removed from the model. Even if the mean radius of the droplets is doubled, no significant change occurs. This can be explained by the examination of the change in total capacitance in relation to the change in droplet radius. With the Electrostatics module of COMSOL Multiphysics® the total capacitance of the device is calculated and shown in Figure 13. By doubling the average radius of the droplets the capacitance rises from 1.825 fF to 1.85 fF. That is an increase of about 1.4 % which is in turn neglible for the cut-off frequency. It can be concluded that these smaller droplets do not need to be considered a problem in the development of the RF device and that the most important factor is to achieve good contact with all cones.

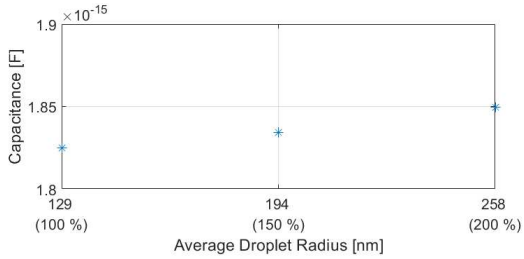

Figure 13: Change of total capacitance depending on average radius of droplets.

Conclusion

This work demonstrates a method, how nanostructures from SEM images can be reproduced as true digital 3D models. The imitation is based on the stochastic parameters of the geometry formulation. Thus it is possible to create random surfaces that have the same properties as the surfaces of the SEM images. These models can be further used in a simulation program like COMSOL Multiphysics® to optimize the structures in their shape and design. In this paper the randomly generated surfaces were used to model Schottky diode structures which are suitable as high frequency rectifiers and to maximize their cut-off frequencies. The proposed model allows for the first time to reliably estimate the optimal shape, size and density of the underlying conical nanostructures with respect to a maximal RF performance.

*This work was supported by the German Research Foundation DFG in the project Flexible Radio Frequency Identification Tags and Systems (FlexID).

References

[1] L. Kuehnel, D. Pandel, R. Schmechel, J. Moeller, K. Neumann, A. Rennings, D. Erni, A. Hierzenberger, M. Schleberger, O. J. Nguon, J. Duvigneau. G. J. Vancso, and N. Benson, "Silicon nanoparticle inks for rf electronic applications," presented at the FLEX Europe 2017/SEMICON Europa 2017, Nov. 15-16, Munich, Germany, session 3 'Materials Advancement', 2017.

[2] M. A. Hernández-Fenollosa, D. Cuesta-Frau, L. C. Damonte, and M. A. Satorre Aznar, "Structural characterisation of semiconductors by computer methods of image analysis," in *Proc. SPIE*, vol. 5878, 2005.

[3] Z. Lu, X. Hu, and Y. Lu, "Particle morphology analysis of biomass material based on improved image processing method," *International Journal of Analytical Chemistry*, vol. 2017, Article ID 5840690, 9 pages, 2017.

[4] MathWorks, "Matlab and image processing toolbox release 2018a," Massachusetts, United States. [Online]. Available: https://mathworks.com

[5] R. M. Haralick, S. R. Sternberg and X. Zhuang, "Image analysis using mathematical morphology," vol. 9, pp. 532–550, 1987.

[6] R. C. Gonzalez and R. E. Woods, *Digital image processing 3rd ed.* Upper Saddle River N.J.: Prentice Hall, 2008.

[7] J. Canny, "A computational approach to edge detection," *IEEE Trans. Pattern Anal. Mach. Intell.*, vol. 8, no. 6, pp. 679–698, 1986.

[8] N. D. Arora, J. R. Hauser, and D. J. Roulston, "Electron and hole mobilities in silicon as a function of concentration and temperature," *IEEE Trans. Electron Devices*, vol. 29, no. 2, pp. 292–295, 1982.

[9] K. S. Champlin and G. Eisenstein, "Cutoff frequency of submillimeter schottky-barrier diodes," *IEEE Trans. Microw. Theory Techn.*, vol. 26, no. 1, pp. 31–34, 1978.